Finite Element Analysis of Fluid Flows with Moving Boundary

Kyung Se Cha*
Graduate School, Department of Mechanical Engineering, Chonnam National University, Kwangju 500-757, Korea
Jong Wook Choi
School of Mechanical and Automotive Engineering, Sunchon National University, Sunchon 540-742, Korea
Chan Guk Park
Professor, Department of Mechanical Engineering, Chonnam National University, Kwangju 500-757, Korea

The objective of the present study is to analyze the fluid flow with moving boundary using a finite element method. The algorithm uses a fractional step approach that can be used to solve low-speed flow with large density changes due to intense temperature gradients. The explicit Lax-Wendroff scheme is applied to nonlinear convective terms in the momentum equations to prevent checkerboard pressure oscillations. The ALE(Arbitrary Lagrangian Eulerian) method is adopted for moving grids. The numerical algorithm in the present study is validated for two-dimensional unsteady flow in a driven cavity and a natural convection problem. To extend the present numerical method to engine simulations, a piston-driven intake flow with moving boundary is also simulated. The density, temperature and axial velocity profiles are calculated for the three-dimensional unsteady piston-driven intake flow with density changes due to high inlet fluid temperatures using the present algorithm. The calculated results are in good agreement with other numerical and experimental ones.

Key Words: Finite Element Method, Fractional Step Method, Lax-Wendroff Scheme, ALE (Arbitrary Lagrangian Eulerian), Natural Convection Problem, Piston-Driven Flow

Nomenclature

C_p : Specific heat at constant pressure
f_j : Body force in the x_j-direction
n_k : The k-th component of the unit outward normal to Γ
p : Pressure
p^* : Pressure correction
$\hat{p}$: Relative pressure value
T : Temperature
t : Time
$\triangle t$: Time increment
u : Velocity
$\tilde{u}_k$: Velocity of the fluid relative to the moving grid $(=u_k-u_{kg})$
u_{kg} : Grid velocity
$\hat{u}_j$: Prescribed velocity component
W_p : Piston velocity
$\hat{W}$: Velocity of the fluid relative to the moving grid $(=W-W_g)$
W_g : Grid velocity
$z_p(t)$: Current piston position
Γ_1 : The boundary surface at which prescribed velocity boundary conditions are imposed.

* Corresponding Author,
E-mail : chaks@hanmail.net
TEL : +82-62-530-0206; **FAX** : +82-62-530-1689
Department of Mechanical Engineering, Chonnam National University, Kwangju 500-757, Korea. (Manuscript **Received** May 23, 2001; **Revised** February 22, 2002)

Γ_2 : The boundary surface at which natural boundary conditions are imposed.
k : The coefficient of thermal conductivity
λ : Second viscosity coefficient $\left(=-\frac{2}{3}\mu\right)$
μ : Fluid viscosity
ρ : Density
ν : Kinematic viscosity coefficient
N_j, N_p, N_T : Weighting function

Superscripts
o : Previous time step.
n : Next time step

Subscripts
i : Dummy variable(i=1, 2, 3)
j : Direction variable(j=1, 2, 3)
k : Dummy variable(k=1, 2, 3)

1. Introduction

Numerical simulation of fluid flows with moving boundary has attracted much attention because of their engineering significance. Many investigators have presented various algorithms for analysis of fluid flow problems with moving boundary. Ikegawa et al. (1994) presented FEM/FDM composite scheme to analyze the flow around moving bodies. Kim et al. (1993) presented numerical methodology for moving boundary problems occurring in axisymmetric coordinate systems. Hirt et al. (1970) proposed the Lagrangian method to deal with transient two-dimensional incompressible viscous flow with free surface. Ramaswamy et al. (1986) used the Lagrangian finite element method for the analysis of two-dimensional sloshing problems. To avoid the shortcomings associated with a severe distortion of mesh in the Lagrangian methods, ALE (Arbitrary Lagrangian Eulerian) method has been proposed by Hirt et al. (1974). The ALE method allows the velocity of the fluid relative to the moving grid. Ramaswamy and Kawahara (1987) and Choi(1996) analyzed the propagation of a solitary wave. Huerta and Liu(1988) and Soulaimani and Saad(1998) applied the ALE method to various flow problems with free surface.

For piston-driven intake flow in a pipe assembly containing a sudden expansion, Pereria(1986) divided the calculation domain into two subdomains, the inlet pipe and the in-cylinder region, respectively. The computations were then performed by two different computer codes. But disadvantage of this calculation procedure is the neglect of the backward influence of the pressure at the sudden expansion. So Ströll et al. (1993) using the finite volume method, calculated simultaneously the flow in the whole region and compared the numerical results with experimental ones.

The objective of the present research is to develop and test a practical numerical algorithm for analysis of fluid flow problems with moving boundary. The present numerical scheme employs an explicit, fractional step method(Donea et al., 1982, Ramaswany, 1988, Codina et al., 1998, Folch et al., 1999) which allows the use of equal interpolation spaces for the pressure and velocity fields and can be used to solve low-speed flow with large density changes due to intense temperature gradients. The explicit Lax-Wendroff scheme for the nonlinear convective terms is used to prevent the checkerboard pressure oscillations of the other equal order interpolation methods. This scheme is second order accurate in time and has a streamline character, which is provided directly by this method without introducing any special upwind mechanism or the introduction of special parameters(Akin, 1994). To treat the moving boundary, the ALE(Arbitrary Lagrangian-Eulerian) method is used in the present study. To validate the numerical algorithm used in the present study, the numerical simulations are performed on several problems including the two-dimensional unsteady flow such as the driven cavity flow and natural convection problem. And in order to extend the present numerical method to the engine simulations, the three-dimensional unsteady flow generated by an impulsively started piston movement in a piston-cylinder assembly is also investigated. By comparing the calculated results with the other numerical and experimental ones, the validity of the

numerical algorithm used in the present study has been confirmed. Furthermore, the density, temperature and axial velocity profiles are calculated for the three-dimensional unsteady piston-driven intake flow with density changes due to high inlet fluid temperatures using the present algorithm.

2. Governing Equations

The fluid flow is modeled with the Navier-Stokes equations that contain the conditions of conservation of mass, momentum and energy. These equations can be written as the continuity equation.

$$\frac{\partial \rho}{\partial t}+\frac{\partial}{\partial x_k}(\rho \tilde{u}_k)=0 \tag{1}$$

the momentum equation.

$$\rho\frac{\partial u_j}{\partial t}+\rho\tilde{u}_k\frac{\partial u_j}{\partial x_k}=-\frac{\partial p}{\partial x_j}+\frac{\partial}{\partial x_j}\left(\lambda\frac{\partial u_k}{\partial x_k}\right)+\frac{\partial}{\partial x_i}\left[\mu\left(\frac{\partial u_i}{\partial x_j}+\frac{\partial u_j}{\partial x_i}\right)\right]+\rho f_j \tag{2}$$

and the energy equation.

$$\rho C_p\frac{\partial T}{\partial t}+\rho C_p\tilde{u}_k\frac{\partial T}{\partial x_k}=\frac{\partial}{\partial x_j}\left(k\frac{\partial T}{\partial x_j}\right)+\Phi$$
$$\left(\Phi=\frac{\partial p}{\partial t}+\tilde{u}_k\frac{\partial p}{\partial x_k}+\lambda\left(\frac{\partial u_k}{\partial x_k}\right)^2+\mu\left(\frac{\partial u_i}{\partial x_j}+\frac{\partial u_j}{\partial x_i}\right)\frac{\partial u_j}{\partial x_i}\right) \tag{3}$$

For ideal gas, the equation of state is defined as

$$p=\rho RT \tag{4}$$

In these equations, $\tilde{u}_k=u_k-u_{kg}$ is the velocity of fluid relative to the moving grid, u_k is the local velocity components and u_{kg} is the grid velocity.

3. Finite Element Formulation

The spatial domain is discretized with eight-node isoparametric hexahedral elements. The density is piecewise constant within an element and is defined at the centroid of each element. The governing equations can be separated into convection, viscosity and pressure terms by the fractional step method and these equations are discretized using the well known Galerkin method. At first we consider only the convective terms in the momentum equation.

$$\rho\frac{\partial u_j}{\partial t}+\rho\tilde{u}_k\frac{\partial u_j}{\partial x_k}=0 \tag{5}$$

Equation (5) is discretized in time by considering a Taylor-series expansion in the time step $\triangle t$, up to second-order to use the explicit Lax-Wendroff scheme for the nonlinear convective terms. Multiplying this by a weighting function N_j, integrating the second order spatial derivatives terms by parts, and using the divergence theorem, the weak form of this stage can be stated as follows:

$$\begin{aligned}\int_\Omega N_j u_j^c\,d\Omega=&\int_\Omega N_j u_j^o\,d\Omega-\triangle t\int_\Omega N_j\tilde{u}_k^o\frac{\partial u_j^o}{\partial x_k}d\Omega\\&-\frac{\triangle t^2}{2}\left(\int_\Omega N_j\tilde{u}_i^o\frac{\partial \tilde{u}_k^o}{\partial x_k}\frac{\partial u_j^o}{\partial x_i}d\Omega+\int_\Omega\frac{\partial N_j}{\partial x_k}\tilde{u}_k^o\tilde{u}_i^o\frac{\partial u_j^o}{\partial x_i}d\Omega\right)\\&+\frac{\triangle t^2}{2}\int_\Gamma N_j\tilde{u}_k^o\tilde{u}_i^o\frac{\partial u_j^o}{\partial x_i}n_k d\Gamma\end{aligned} \tag{6}$$

This convection step allows us to determine an intermediate velocity field u^c from u^o. On the boundary of the domain Ω we have the following boundary conditions.

$$u_j^c=\hat{u}_j(x_1,\ x_2,\ x_3)\ \text{ on }\ \Gamma_1 \tag{7}$$

If no-slip condition is imposed at the boundary, the value of u_j^c is zero.

Now we consider the viscosity and body force terms in the momentum equation.

$$\rho\frac{\partial u_j}{\partial t}=\frac{\partial}{\partial x_j}\left(\lambda\frac{\partial u_k}{\partial x_k}\right)+\frac{\partial}{\partial x_i}\left[\mu\left(\frac{\partial u_i}{\partial x_j}+\frac{\partial u_j}{\partial x_i}\right)\right]+\rho f_j\qquad\left(\lambda=-\frac{2}{3}\mu\right) \tag{8}$$

Where λ and f_j denote the second viscosity coefficient and the body force. The weak formulation can be written as follows:

$$\begin{aligned}\int_\Omega N_j u_j^\nu\,d\Omega=&\int_\Omega N_j u_j^c\,d\Omega-\triangle t\nu\int_\Omega\frac{\partial N_j}{\partial x_i}\frac{\partial u_j^c}{\partial x_j}d\Omega\\&-\frac{1}{3}\triangle t\nu\int_\Omega\frac{\partial N_j}{\partial x_j}\frac{\partial u_k^c}{\partial x_k}d\Omega+\triangle t\int_\Omega N_j f_j d\Omega\\&+\triangle t\nu\int_\Gamma N_j\frac{\partial u_i^c}{\partial x_i}n_i d\Gamma+\triangle t\nu\int_\Gamma N_j\frac{\partial u_j^c}{\partial x_i}n_i d\Gamma\\&-\frac{2}{3}\triangle t\nu\int_\Gamma N_j\frac{\partial u_k^c}{\partial x_k}n_j d\Gamma\end{aligned} \tag{9}$$

Where u^c denotes the result from Eq (6). Here, a new intermediate velocity u^ν is determined from u^c. The boundary conditions in the viscosity

terms are the same those in the convective terms. In this procedure, the intermediate velocity does not generally satisfy the continuity constraint, therefore we must account for this in the pressure calculation. To compute the pressure, we employ the pair of equations.

$$\frac{\partial \rho}{\partial t}+\frac{\partial}{\partial x_k}(\rho u_k)=0 \tag{10}$$

$$\rho\frac{\partial u_j}{\partial t}=-\frac{\partial p}{\partial x_j} \tag{11}$$

Eq. (10) and Eq. (11) are descretized in time as follows:

$$\frac{\rho^n-\rho^o}{\Delta t}+\frac{\partial}{\partial x_k}(\rho u_k{}^n)=0 \tag{12}$$

$$\frac{\rho u_j{}^n-\rho u^\nu}{\Delta t}=-\frac{\partial p^n}{\partial x_j} \tag{13}$$

Let us introduce the pressure p^n as:

$$p^n=p^o+p^* \tag{14}$$

Where p^* denotes pressure correction. Using the Eq. (14), Eq. (13) can be separated into two equations.

$$\frac{\rho u_j{}^n-\rho u_j^*}{\Delta t}=-\frac{\partial p^*}{\partial x_j} \tag{15}$$

$$\frac{\rho u_j^*-\rho u_j^\nu}{\Delta t}=-\frac{\partial p^o}{\partial x_j} \tag{16}$$

We first compute intermediate velocity field u^* using the previous values from Eq. (16). After taking the gradient of Eq. (15), and using the Eq. (12), we obtain the equation for pressure correction as follows:

$$\frac{\partial^2 p^*}{\partial x_j{}^2}=\frac{1}{\Delta t}\left(\frac{\rho^n-\rho^o}{\Delta t}+\frac{\partial(\rho u_j^*)}{\partial x_j}\right) \tag{17}$$

Multiplying by a weighting function N_p, integrating over Ω and integrating the second order spatial derivatives terms by parts, and using the divergence theorem, the weak form of Eq. (17) can be written as

$$\begin{aligned}&\int_\Gamma N_p\frac{\partial p^*}{\partial x_j}n_j d\Gamma-\int_\Omega\frac{\partial N_p}{\partial x_j}\frac{\partial p^*}{\partial x_j}d\Omega\\&=\frac{1}{\Delta t}\int_\Omega N_p\frac{\partial(\rho^n u_j^*)}{\partial x_j}d\Omega\\&\quad+\frac{1}{\Delta t^2}\int_\Omega N_p(\rho^n-\rho^o)\,d\Omega\end{aligned} \tag{18}$$

The first term vanishes since we have $\frac{\partial p}{\partial n}=0$ on Γ for the correction term. To solve Eq. (17), the following conditions are applied.

$$\frac{\partial p}{\partial n}=\vec{n}\cdot\frac{[\vec{u^\nu}-\vec{u^n}]}{\Delta t} \text{ on } \Gamma_1 \tag{19}$$

$$p=\hat{p}(x_1, x_2, x_3) \text{ on } \Gamma_2 \tag{20}$$

Once the pressure correction p^* has been determined from Eq. (18), nodal velocities u^n can be computed from the weak form of Eq. (15).

$$\int_\Omega N_p u_j^n d\Omega=\int_\Omega N_p u_j^* d\Omega-\frac{\Delta t}{\rho}\int_\Omega N_p\frac{\partial p^*}{\partial x_j}d\Omega \tag{21}$$

The boundary conditions in the velocity correction terms are the same those in the convective and viscous terms.

Let us now consider energy Eq. (3) using the methods similar to those of momentum equations. The weak form of Eq. (3) can be separated into convection and viscosity terms as follows:

$$\begin{aligned}\int_\Omega N_T T^c d\Omega=&\int_\Omega N_T T^o d\Omega-\Delta t\int_\Omega N_T\tilde{u}_k^n\frac{\partial T^o}{\partial x_k}d\Omega\\&-\frac{\Delta t^2}{2}\int_\Omega N_T\tilde{u}_i^n\frac{\partial\tilde{u}_k^n}{\partial x_k}\frac{\partial T^o}{\partial x_i}d\Omega\\&-\frac{\Delta t^2}{2}\int_\Omega\frac{\partial N_T}{\partial x_k}\tilde{u}_k^n\tilde{u}_i^n\frac{\partial T^o}{\partial x_i}d\Omega\\&+\frac{\Delta t^2}{2}\int_\Gamma N_T\tilde{u}_k^n\tilde{u}_i^n\frac{\partial T^o}{\partial x_i}n_k d\Gamma\end{aligned} \tag{22}$$

$$\begin{aligned}\int_\Omega N_T T^n d\Omega=&\int_\Omega N_T T^c d\Omega-\alpha\Delta t\int_\Omega\frac{\partial N_T}{\partial x_j}\frac{\partial T^c}{\partial x_j}d\Omega\\&+\frac{\Delta t}{\rho C_p}\int_\Omega N_T\Phi d\Omega\\&+\alpha\Delta t\int_\Gamma N_T\frac{\partial T^c}{\partial x_j}n_j d\Gamma\end{aligned} \tag{23}$$

Once the weak forms of differential equations have been established, all variables interpolated by the linear shape functions are substituted into the weak forms of differential equations and then these equations can be integrated spatially by Gauss numerical integration formula. In the Galerkin method, all the weighting functions N_j, N_p and N_T are the same as the shape functions.

To obtain a simple and efficient solution algorithm for calculating the variables, it is attractive to replace the consistent mass matrix by a diagonal mass matrix. The most common solution to defining a diagonal matrix is to lump, or sum, all the terms in a given row onto the diagonal of the row and then set the off-diagonal terms zero.

That is, the lumped matrix M_L^e is defined such that

$$M_{Lij}^e=0 \text{ if } i\neq j,$$
$$M_{Lii}^e=\sum_j M_{ij}^e \tag{24}$$

Another diagonal matrix, M_{Dij}^e which is called the diagonalized matrix is defined such that

$$M_{Dij}^e=0 \text{ if } i\neq j,$$
$$M_{Dii}^e=M_{ii}^e\left(\sum_i\sum_j M_{ij}^e/\sum_i M_{ii}^e\right) \tag{25}$$

For linear simplex elements in two and three dimensions both procedures yield identical diagonal matrices. However, for axisymmetric problems and higher order elements they yield different results and the diagonalized matrix appears to be best in general(Akin, 1994). This is because for higher order elements the lumped form can introduce zeros or negative numbers on the diagonal. In the present study, we use the diagonalized matrix for converting the consistent mass matrix to a diagonal matrix.

4. Numerical Examples

4.1 Lid-driven cavity problem

As first application example of the method proposed in the present study, the driven cavity

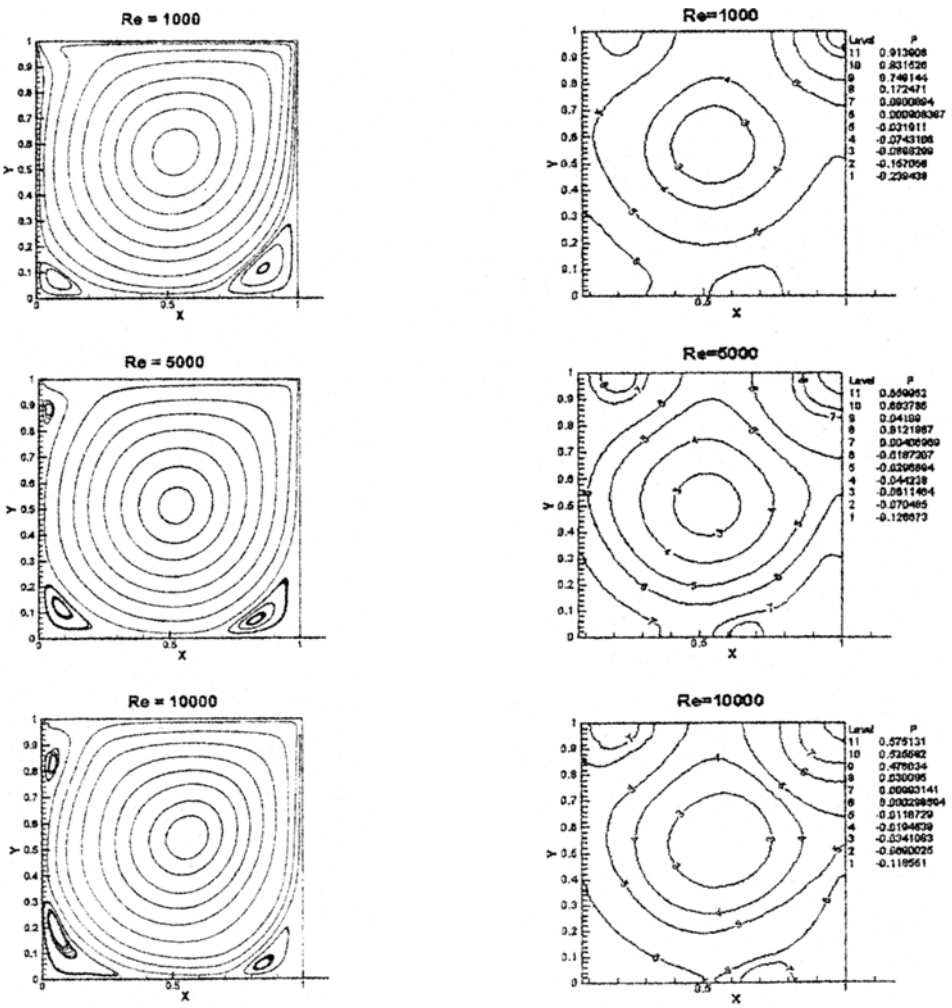

(a) Streamlines (b) Pressure contours

Fig. 1 Streamlines and pressure contours at steady state

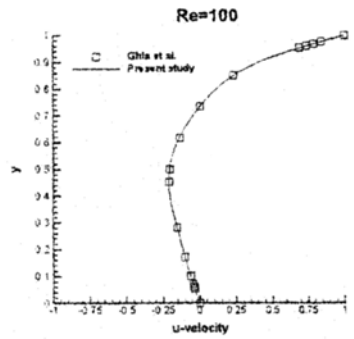

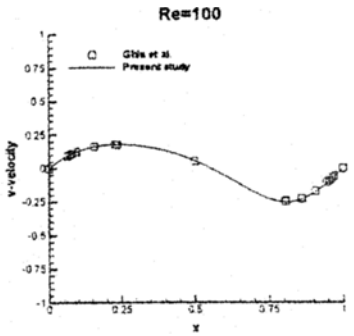

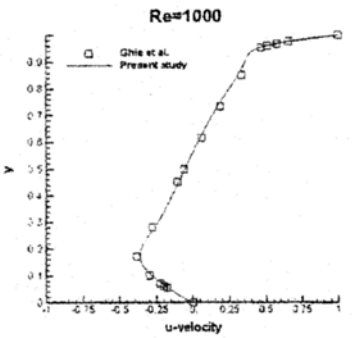

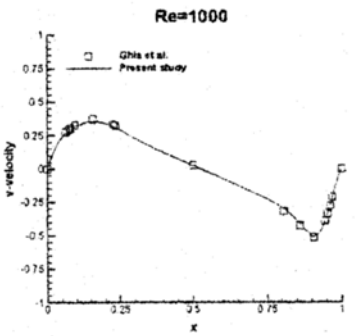

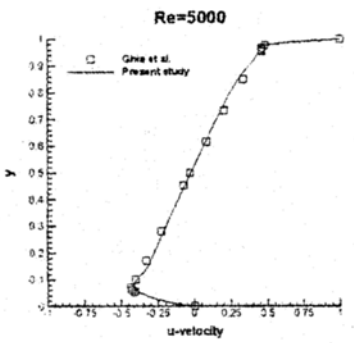

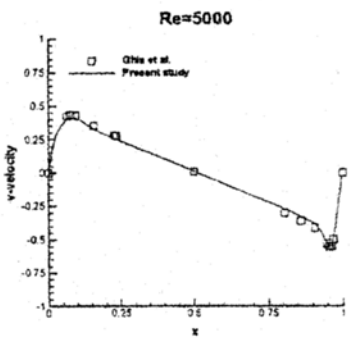

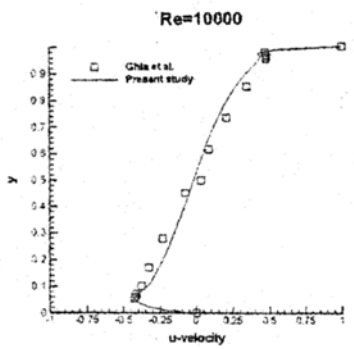

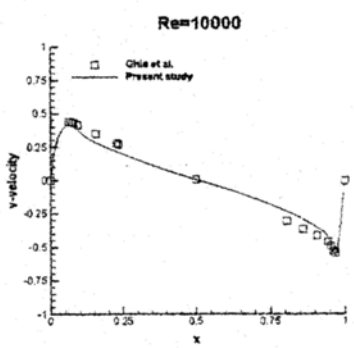

(a) Velocity component along x-coordinate (b) Velocity component along y-coordinate

Fig. 2 Velocity profiles for cavity flow

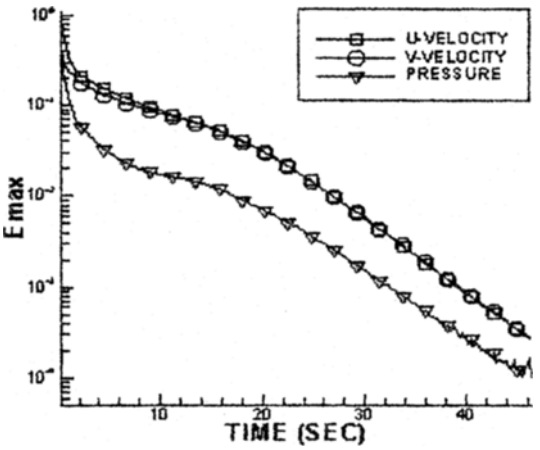

Fig. 3 Convergence history for Re=1000

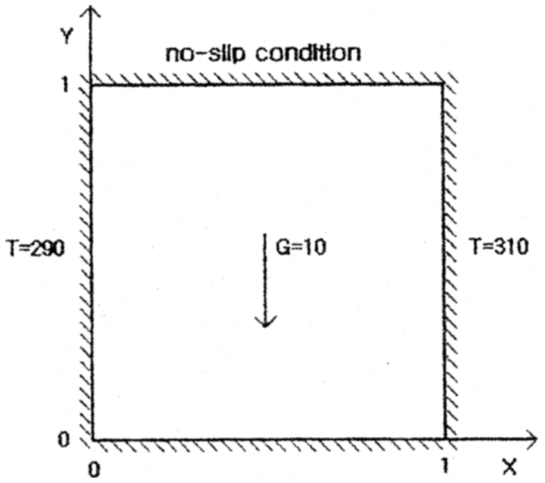

Fig. 4 Boundary conditions for natural convection problem

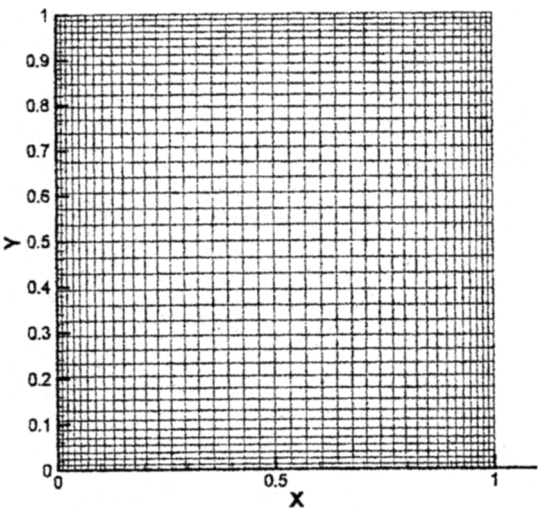

Fig. 5 Nonuniform 41×41 grid system for natural convection problem

problem with a top surface moving at a constant velocity is presented. The calculations were performed on the nonuniform 41×41 grid structure for the Reynolds numbers of 100, 1000, 5000, and 10000. The Reynolds numbers are based on the length of the square cavity and the velocity of the moving wall. No-slip boundary conditions were specified in all boundaries except on the top surface. A pressure datum, $p=0$, was specified at the middle of the bottom wall.

We obtained a converged solution for each case with trivial initial guess of $u=v=p=0$. The steady state solution is obtained when the following condition is satisfied:

$$E_{\max}=\max \mid \phi^{n}{}_{i}-\phi^{n-1}{}_{i} \mid <10^{-4} \qquad (26)$$

where the subscript i denotes the specific node point, the superscript n denotes the time level, and ϕ denotes the normalized variable. Figure 1 show the streamlines and the pressure contours at steady state. The profiles of the dimensionless x-direction velocity along the vertical centerline of the driven cavity (x=0.5) and the dimensionless y-direction velocity along the horizontal centerline of the driven cavity (y=0.5) are illustrated for various Reynolds numbers in Fig. 2. These results are compared with those of Ghia et al. (1982) obtained with a 129×129 grid via a multigrid technique. Good agreement can be found for both maximum velocity position and value at Re=100, 1000, 5000 and 10000. Figure 3 shows the convergence history for Re=1000. A time increment $\triangle t=0.1$ is used in this problem.

4.2 Natural convection in a square cavity

A natural convection problem is considered in this section. The flow domain and boundary conditions for this problem are shown in Fig. 4. We discretized the domain into a mesh of 40×40 elements with smaller elements close to the boundary to capture the boundary layers, see Fig. 5. The initial condition is given as: $p=10^{5}$, temper-

ature $\theta=300$ and velocity $u=v=0$ and the fluid properties are assumed to be constant, $R=286$, $c_v=715$, $k=1.0$ and $\mu=0.001$. The Rayleigh number of this problem is $Re\approx 6.5\times 10^5$. We regard the fluid flow as compressible flow in this problem because the density is changed due to temperature differences in a square cavity.

The results of the problem using the present algorithm are shown in Fig. 6 and Fig. 7. The calculated y-direction velocity and temperature distribution along y=0.5 are plotted in Fig. 8 and Fig. 9. The solution by Hendriana and Bathe (2000) using the parabolic quadrilateral finite element method for compressible flows and the

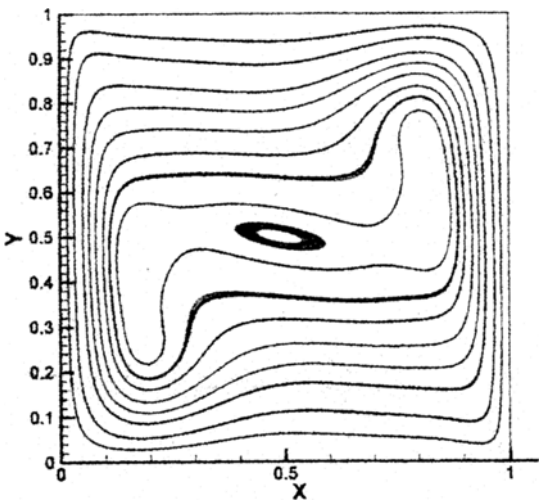

Fig. 6 Streamlines for natural convection problem

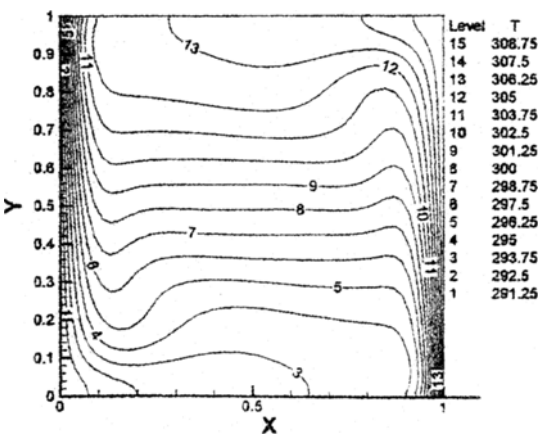

Fig. 7 The temperature distribution for natural convection problem

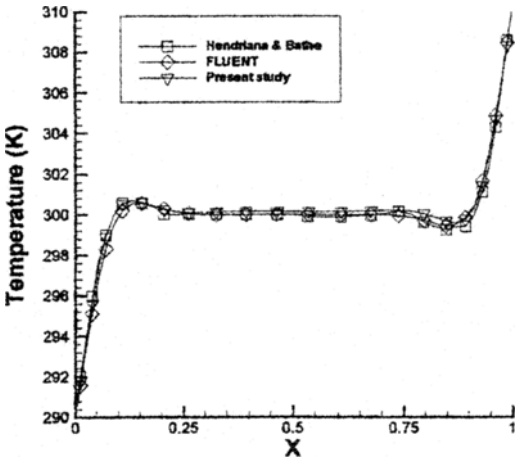

Fig. 8 The temperature values along y=0.5

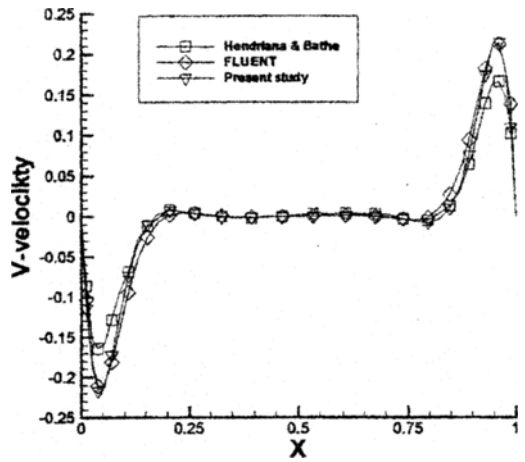

Fig. 9 The y-direction velocity values along y=0.5

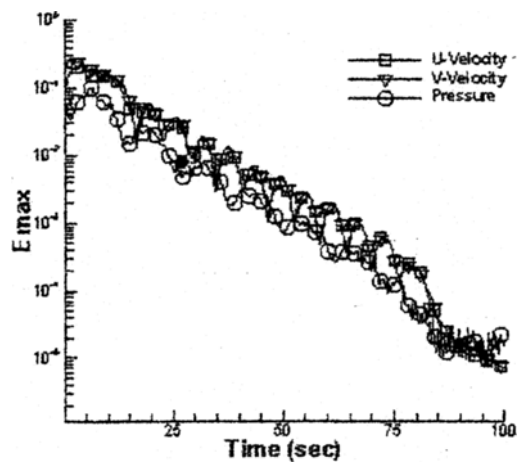

Fig. 10 Convergence history for the natural convection problem

solution using FLUENT are also plotted for comparison. From Fig. 8 and Fig. 9, the results of temperature distributions are close to one another. However, considering the results of y-direction velocity, we see that the present results are closer to the FLUENT solution than Hendriana's solution. Figure 10 shows the convergence history for a natural convection in a square cavity. In the present study, the time increment is $\triangle t=0.1$.

4.3 Piston-driven intake flow

To demonstrate the applicability of the present numerical algorithm on moving grid system, we consider the piston-driven intake flow in a pipe assembly containing a sudden expansion. The piston-cylinder assembly is shown in Fig. 11. The piston position $Z_p(t)$ varies between the initial clearance ($Z_{p,0}$=0.04m) and the maximum displacement (Z_p, max=0.0643m) as a function of time. The piston moves with constant velocity W_p=11.9mm/s. The fluid used was a mixture of dibutylphtalate and Diesel oil. The mesh used for the computation consists of non-uniform 6080 finite elements, which is shown in Fig. 12. While the grid inside the inlet tube remained unchanged with time, the control volumes within the piston chamber were stretched in z-direction. No-slip boundary conditions were specified in all boundaries except the piston surface for the velocities. Along the piston surface the axial velocity component of fluid, W, was set equal to the piston velocity W_p. At the inlet plane the radial velocity components U and V were set to zero and the W-velocity profile was taken uniform, satisfying the global continuity requirement as determined by the piston velocity W_p. The velocity of the fluid relative to the moving grid is $\tilde{W}=W-W_g$ and W_g is the grid velocity, which can be expressed as follows:

$$W_g(Z,\ t)=-\frac{Z}{Z_p(t)}\frac{dZ_p(t)}{dt}, \qquad 0.1\text{m}<Z\leq Z_p(t) \tag{27}$$

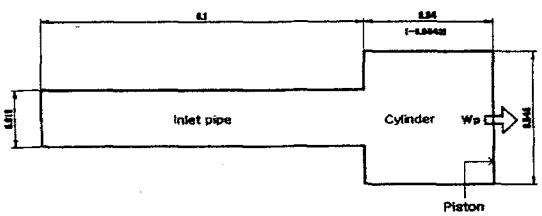

Fig. 11 Piston-cylnder configuration

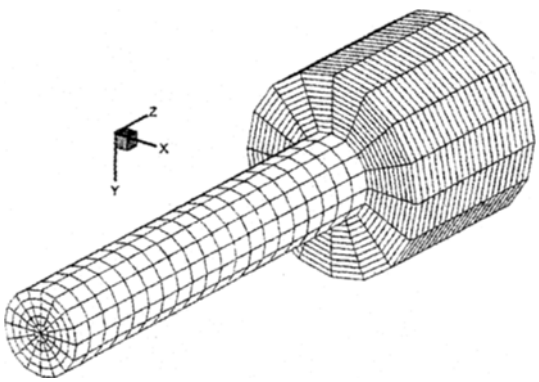

Fig. 12 The mesh used for pistion-driven intake flow

Fig. 13 Streamlines obtained by 3-D FEM

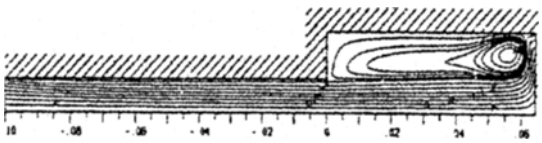

Fig. 14 Streamlines obtained by 2-D FVM

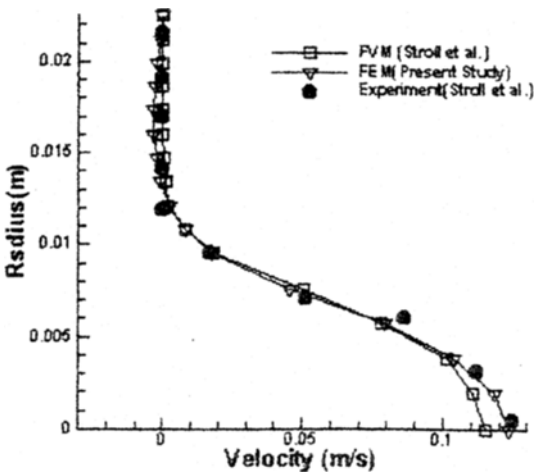

Fig. 15 Axial velocity profiles for z=0.1070(m)

Temperature was not considered in this problem. For the maximum piston displacement (Z_p, max=0.0643m), the predicted streamlines are shown in Fig. 13. For comparison, the solution by Ströll et al. (1993) using a finite volume method is also shown in Fig. 14. From Fig. 13 and Fig. 14, we see that the present results are close to the prediction presented by Ströll et al. Also, the predicted axial velocity profiles at successive z-locations inside the cylinder are compared with the numerical and the experimental data(Ströll, 1993) in Fig. 15, Fig. 16 and Fig. 17. The present results are in good agreement with experimental data. Furthermore, the piston-driven flow with density changed due to high inlet fluid temperatures are considered. The fluid used was air and the calculations were performed for inlet fluid temperature T_{inlet}=300K, 400K and 550K, respectively. All the temperatures in the computational domain except inlet boundary were initially set to 300K. The calculated streamlines with inlet temperature of 550K at several time instances are shown in Fig. 18. As the piston moves to the right, the hot air is sucked through the inlet pipe into the cylinder and it is separated at the sudden expansion, forming a counterclockwise rotating toroidal vortex. As can be also seen from Fig. 18, the vortex is convected towards the piston surface and is elongated with increasing piston displacement. For several z-locations described in Fig. 19, the calculated density and temperature profiles at t=2.0s are shown in Fig. 20, Fig. 21 and Fig. 22. The results show rather intense temperature and density gradients as inlet fluid temperature is increased. Normally for isothermal flows of compressible fluids if the Mach number is smaller than about 0.3, then

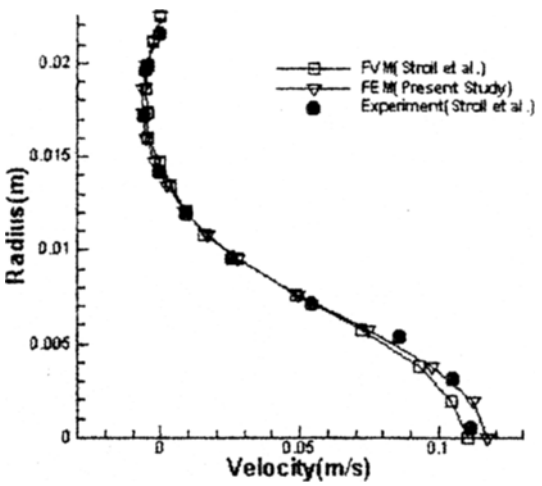

Fig. 16 Axial velocity profiles for z=0.1279(m)

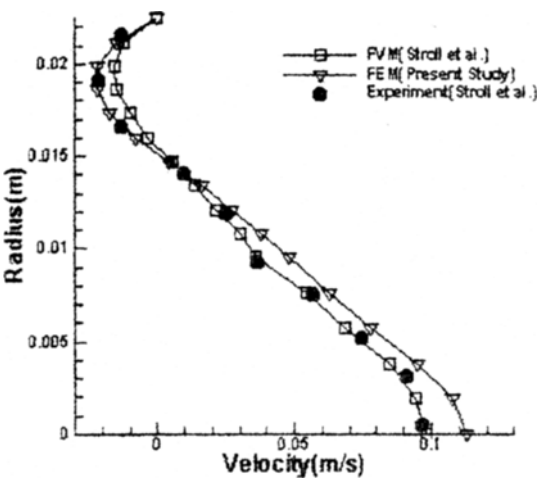

Fig. 17 Axial velocity profiles for z=0.1513(m)

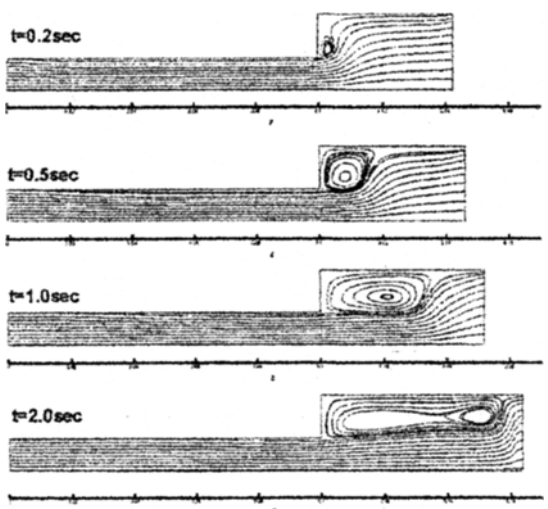

Fig. 18 Streamlines at t=0.2s, 0.5s, 1.0s and 2.0s

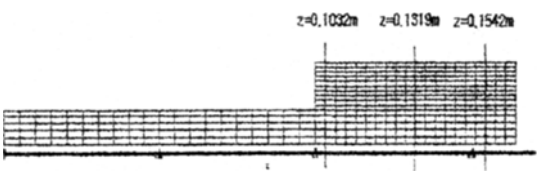

Fig. 19 Positions of the cross-section

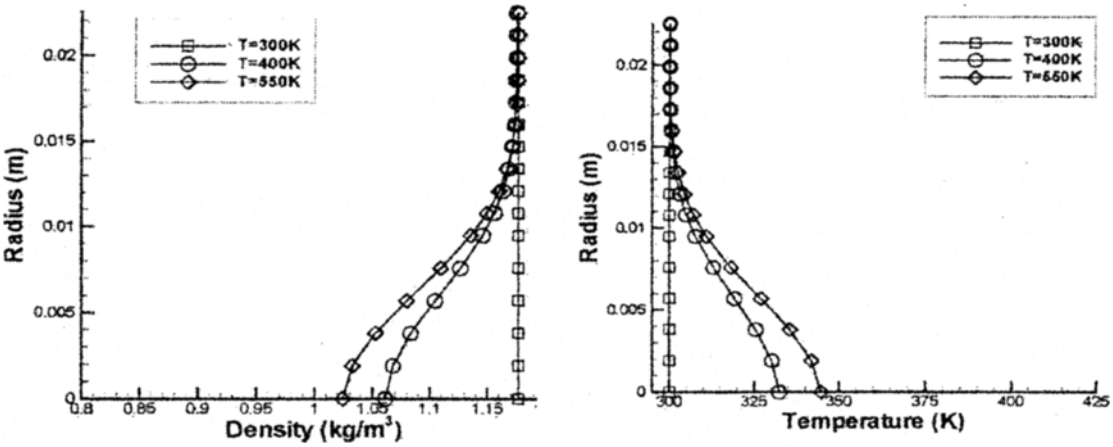

Fig. 20 Density and temperature profiles at z=0.1032m

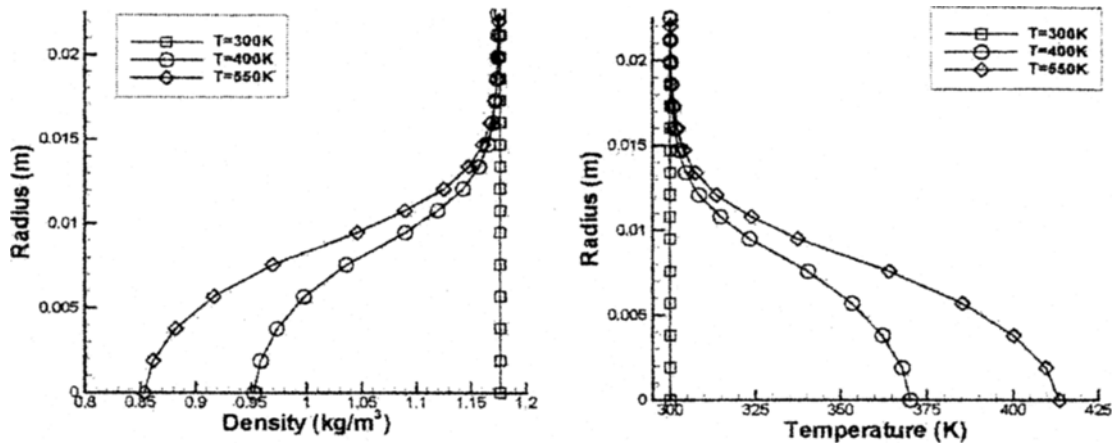

Fig. 22 Density and temperature profiles at z=0.1319m

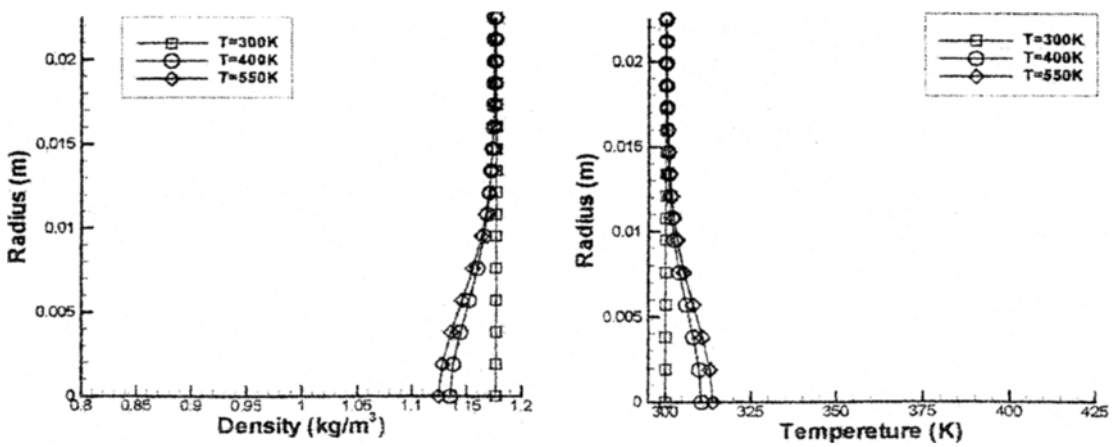

Fig. 22 Density and temperature profiles at z=0.1542m

pressure gradients are small enough so that the density is nearly constant, and the flow may be assumed incompressible. However, for the present problem, large density changes occur due to high inlet fluid temperatures, so that the flow must be assumed compressible.

5. Conclusion

In this paper, we have presented a numerical algorithm which used a fractional step method with equal-order interpolation functions for the velocity components and pressure. The explicit Lax-Wendroff scheme was applied to the non-linear convective terms in the momentum equations and the ALE(Arbitrary Lagrangian-Eulerian) method was adopted for treating the moving boundary. To validate the present algorithm, several problems have been calculated and compared with other results. As a result, the calculation results have shown good agreement with other results. In order to extend the present numerical method to engine simulations, we also investigated the basic behavior of the unsteady flow generated by an impulsively started piston movement in a piston-cylinder assembly, yielding flow separation and spatially moving vortices. The numerical results indicate that the present calculation procedure can be used to predict the behavior of periodic intake/exhaust flows and is applicable to a wide range of problems. Although the discussion has been restricted to laminar flows governed by the Navier-Stokes equations, the methodology proposed can readily be extended to accommodate the Reynolds-averaged equations and turbulence models.

Acknowledgements

This work is sponsored by the Brain Korea 21 Project in 2001. The authors would like to thank for this support.

References

Akin, J. E., 1994, *Finite Elements for Analysis and Design*, Academic Press Limited.

Choi, H. G., 1996, "A Study on Segregated Finite Element Algorithms for the Navier-Stokes Equations," Ph. D. Thesis, Seoul National University.

Codina, R., Vazquez. M. and Zienkiewicz. O. C., 1998, "A General Algorithm for Compressible and Incompressible Flows. Part Ⅲ : The Semi-Implicit Form," *Internat. J. Numer. Methods In Fluids*, Vol. 27, pp. 13～32.

Donea, J., Giuliani. S, Laval. H. and Quartapelle, L., 1982, "Finite Element Solution of the Unsteady Navier-Stokes Equation by a Fractional Step Method," *Comput. Methods Apply. Mech. Engrg.* Vol. 30, pp. 349～388.

Folch, A., Vazquez, M., Codina, R. and Marti. J., 1999, "A Fractional-Step Finite-Element Method for the Navier-Stokes Equations Applied to Magma-Chamber withdrawal," *Computer & Geosciences*, Vol. 25, pp. 263～275.

Ghia, U., Ghia, K. N. and , Shin, C. T., 1982, "High-Re Solutions for Incompressible Flow Using the Navier-Stokes Equations and a Multigrid Method," *J. Comp. Phys.*, Vol. 48, pp. 387～411.

Hendriana, D. and Bathe, K. J., 2000, "On a Parabolic Quadrilateral Finite Element for Compressible Flow," *Comput. Methods Appl. Mech. Engrg.* Vol. 186, pp. 1～22.

Hirt, C. W., Cook, J. L. and Butler, T. D., 1970, "A Lagrangian Method for Calculating the Dynamics of an Incompressible Fluid with Free Surface," *J. Comput. Phys.*, Vol. 5, pp. 103～124,

Hirt, C. W., Amsden, A. A. and Cook, J. L., 1974, "An Arbitrary Lagrangian-Eulerian Computing Method for All Flow Speeds," *J. Comput. Phys.*, Vol. 14, pp. 227～253.

Huerta, A. and Liu, W. K., 1988, "Viscous Flow with Large Free Surface Motion," *Comput. Methods Appl. Mech. Engrg.*, Vol. 69, pp. 277～324.

Ikegawa, M., Kaiho, M. and Kato, C., 1994, "FEM/FDM Composite Scheme for Viscous Incompressible Flow Analysis," *Computer Methods in Applied Mechanics and Engineering*, Vol. 112, pp. 149～163.

Kim., C. J., Ro, S. T. and Lee, J. S., 1993, "An Effective Algorithm to Solve Moving Boun-

dary Problems in Axisymmetric Coordinate Systems," *Transactions of KSME*, Vol. 17, No. 3, pp. 670~679.

Pereira, J. C. F., 1986, "Experimentelle und numerische Untersuchungen station rer and instation rer laminarer Str mungen mit Abl sung," Dr.-Ing.-Dissertation, University of Erlangen-Nürnburg, Germany.

Ramaswamy, B., Kawahara, M. and Nakayama, T., 1986, "Lagrangian Finite Element Method for the Analysis of Two-Dimensional Sloshing Problems," *Int. J. Numer. Methods Fluids*, Vol. 6, pp. 659~670.

Ramaswamy, B. and Kawahara, M., 1987, "Arbitrary Lagrangian-Eulerian Finite Element Method for Unsteady, Convective, Incompressible Viscous Free Surface Fluid Flow," *Int. J. Numer. Methods Fluids*, Vol. 7, pp. 1053~1075.

Ramaswany, B., 1988, "Finite Element Solution for Advection and Natural Convection flow," *Comput. Fluids*, Vol. 16, pp. 349~388.

Soulaimani, A. and Saad, Y., 1998, "An arbitrary Lagrangian-Eulerian Finite Element Method for Solving Three-Dimensional Free Flows," *Comput. Methods Appl. Mech. Engrg.*, Vol. 162, pp. 79~106.

Ströll, H., Durst, F., Peric, M., Pereira, J. C. F. and Scheuerer, G., 1993, "Study of Laminar, Unsteady Piston-Cylinder Flows," *ASME Journal of Fluids Engineering*, Vol. 115, pp. 687~693.